



OPEN

Radiocesium in the Taiwan Strait and the Kuroshio east of Taiwan from 2018 to 2019

Wei-Jen Huang^{1✉}, Ming-Ta Lee², Kuei-Chen Huang¹, Kai-Jung Kao¹, Ming-An Lee^{3,4}, Yiing-Jang Yang⁵, Sen Jan⁵ & Chen-Tung Arthur Chen^{1✉}

The release of anthropogenic radiocesium to the North Pacific Ocean (NPO) has occurred in the past 60 years. Factors controlling ¹³⁷Cs (half-life, 30.2 year) and ¹³⁴Cs (half-life, 2.06 year) activity concentrations in the Kuroshio east of Taiwan and the Taiwan Strait (latitude 20° N–27° N, longitude 116° E–123° E) remain unclear. This study collected seawater samples throughout this region and analyzed ¹³⁴Cs and ¹³⁷Cs activity concentrations between 2018 and 2019. A principal component analysis (PCA) was performed to analyze the controlling factors of radiocesium. Results of all ¹³⁴Cs activity concentrations were below the detection limit (0.5 Bq m⁻³). Analyses of water column ¹³⁷Cs profiles revealed a primary concentration peak (2.1–2.2 Bq m⁻³) at a depth range of 200–400 m (potential density σ_θ : 25.3 to 26.1 kg m⁻³). The PCA result suggests that this primary peak was related to density layers in the water column. A secondary ¹³⁷Cs peak (1.90 Bq m⁻³) was observed in the near-surface waters (σ_θ = 18.8 to 21.4 kg m⁻³) and was possibly related to upwelling and river-to-sea mixing on the shelf. In the Taiwan Strait, ¹³⁷Cs activity concentrations in the near-surface waters were higher in the summer than in the winter. We suggest that upwelling facilitates the vertical transport of ¹³⁷Cs at the shelf break of the western NPO.

The global fallout from the atmospheric nuclear weapons tests during the late 1950s to early 1960s is the main source of artificial radiocesium to the world ocean^{1,2} and can still be discerned in the surface water, the sub-surface, and deep waters (up to 600–1000 m) in the western North Pacific Ocean (NPO)³. After the Fukushima Daiichi nuclear power plant (FDNPP) accident on March 11th, 2011, additional anthropogenic radiocesium with long half-life ¹³⁷Cs (30.2 year) and short half-life ¹³⁴Cs (2.06 year) was released into the NPO^{4–11}. Previous studies have estimated that the total amount of ¹³⁷Cs released by the FDNPP accident ranged between 15 and 27 PBq, of which a very significant portion found its way to the atmosphere and ocean^{5,12,13}. Traceable, FDNPP-derived ¹³⁷Cs (latitude 37.42° N, longitude 141.03° E) follows the pathway of the North Pacific circulation toward the eastern NPO^{6,9,14}. Thus 60 years after the first nuclear tests in the Pacific region, the fate of long-lives radionuclides on the western NPO and adjacent marginal seas still raises social concerns about potential health risks, e.g. associated with seafood consumption and fishing industry.

Recent studies have observed that ¹³⁷Cs can disperse through the Subtropical Mode Water (STMW) and Central Mode Water (CMW) in the western NPO^{9,15}. STMW is formed right south of the Kuroshio Current and Extension (between 132° E and near the dateline) by deep vertical convection in winter^{16–18}. CMW forms north of the Kuroshio Extension (around 36–41° N, 160° E–165° W), hence is characterised by colder temperatures and a deeper layer (250–500 m)¹⁹. These two water masses (i.e., STMW and CMW) circulate clockwise beneath the surface of the western NPO²⁰. When plotted against depth, the vertical profiles of ¹³⁷Cs activity concentrations recorded at 20° N, 165° E in 2002 exhibited two distinct peaks: the first one at a potential density (σ_θ) of 25.5 kg m⁻³ (corresponding to the σ_θ range of STMW) and the second one at a σ_θ of 26.0 kg m⁻³ (corresponding to the σ_θ range of CMW)³. The subsequent injection of FDNPP-derived radionuclides resulted in a contamination plume spreading eastward and merging with the Oyashio Current; hence the incorporation of radiocesium in the formation of STMW and CMW and its current value as a tracer of ocean circulation⁴.

Both water masses (i.e., STMW and CMW) extend clockwise to the western boundary of the NPO, where the Kuroshio is most intense. Branches of the Kuroshio Current intrude into the northern South China Sea

¹Department of Oceanography, National Sun Yat-Sen University, Kaohsiung, Taiwan. ²The Radiation Monitoring Center, Atomic Energy Council, Kaohsiung, Taiwan. ³Department of Environmental Biology and Fisheries Science, National Taiwan Ocean University, Keelung, Taiwan. ⁴Center of Excellence for Ocean Engineering, National Taiwan Ocean University, Keelung 20224, Taiwan. ⁵Institute of Oceanography, National Taiwan University, Taipei, Taiwan. ✉email: wjhuang29@mail.nsysu.edu.tw; ctchen@mail.nsysu.edu.tw

(SCS), southern Taiwan Strait, and even the southern East China Sea (ECS). Inomata et al.⁶ estimated that 5.0% of the total amount of FDNPP-derived ¹³⁷Cs in the STMW entered into the Sea of Japan before 2016 through clockwise spreading in the western NPO, ECS, and the Sea of Japan. Several studies have reported the intrusion of radiocesium into the western NPO but also into the adjacent marginal seas after the FDNPP event^{4,5,21}. However, seawater ¹³⁷Cs activity concentrations have hardly been investigated in the Kuroshio east of Taiwan and the Taiwan Strait, particularly after the 2011 event.

Subtropical marginal seas of the western NPO are characterized by a monsoon cycle and seasonal coastal currents. For instance, the Taiwan Strait is affected by the northeasterly monsoon in the winter and the southwesterly monsoon in the summer^{22,23}. As a result, the northern half of the Taiwan Strait is characterized by a southward-flowing coastal current in the winter while the southern half of the Taiwan Strait is characterized by a warm, northward-flowing current reinforced by the Kuroshio intrusion branch in the summer^{24–27}. Furthermore, there are well documented upwelling regions in the study area, such as the waters off northeastern Taiwan^{28,29}, several regions in the Taiwan Strait^{30,31}, and regions in the northern SCS^{32–34}. However, to the best of our knowledge, the effects of seasonality and upwelling on the fate of radiocesium in seawater in this study area remain unclear.

This study reports the activity concentration of ¹³⁴Cs and ¹³⁷Cs over the shelf break of the western NPO and examines the fates of these radionuclides on the shallow continental shelf. The ¹³⁴Cs and ¹³⁷Cs activity concentrations were measured on samples collected in near-surface, subsurface or deeper waters in the Kuroshio region east of Taiwan and the Taiwan Strait between 2018 and 2019. The origin of the ¹³⁷Cs maximum in the subsurface/deep waters and the factors controlling seasonal variations in ¹³⁷Cs activity concentration in the near-surface waters are discussed.

Methods

From 2018 to 2019, surface (< 5 m), subsurface (5–200 m), and deep seawater (200–1000 m) samples were collected at sites in the Kuroshio east of Taiwan and the Taiwan Strait (Fig. 1). Surface seawater samples (40 or 60 L) were collected mostly from fishing boats by using cleaned 20-L tanks. Subsurface samples were taken by using Niskin bottles mounted on a Conductivity–Temperature–Depth (CTD) rosette, which recorded temperature, salinity (from conductivity), and water depth (from pressure) onboard R/Vs Ocean Researcher I, II, and III. Sampling locations are shown in Fig. 1. Each 20-L sample was acidified using hydrochloric acid (11 M HCl, 100 mL) and was kept at room temperature (~ 15–30 °C) until it was transported to the Radian Monitor Center, Atomic Energy Council, Kaohsiung, Taiwan. Radiocesium was pre-concentrated by adsorption onto ammonium molybdophosphate (AMP)^{35,36} and counted using a high-purity germanium (HPGe) detector with lead shielding. Each 40-L or 60-L sample was counted for 200,000 s or 120,000 s, respectively. The detection limits of both ¹³⁴Cs and ¹³⁷Cs were 0.5 Bq m⁻³. In this study, we corrected all ¹³⁷Cs activity concentrations to January 1st, 2020. This date was also applied to data in earlier studies for comparison purposes.

Total alkalinity (TA) samples were collected together with nearly 61% of radiocesium samples (92% of 49 subsurface and deep waters, and 55% of 242 near-surface waters). TA water samples were taken into 250-mL borosilicate glass bottles and poisoned immediately with 100-μL saturated HgCl₂ solution to eliminate biological activities. We followed the open-cell Gran titration method with a temperature-controlled, semi-automated titrator (AS-ALK2 Apollo Scitech) to determine TA value of each sample. TA measurements were referenced against certified reference materials from A. G. Dickson's laboratory at Scripps Institution of Oceanography with a precision of 0.1%³⁷. TA is usually treated as a conservative tracer. We used it to determine the water sources and possible mixing processes between fresh water and seawater by normalizing TA values to salinity 35 (NTA = (TA/S) × 35)³⁸.

As variables can be collectively controlled by major oceanographic mechanisms, principal component analysis (PCA)^{39,40} serves as a multivariate analysis tool to catch the major features of a dataset. PCA can analyze inter-correlations among these variables and reduces the dimension of a dataset. The major factors affecting this dataset is thus obtained. The result is displayed as a subset of new, independent (orthogonal) variables which are referred to as dimensions. The higher the coordinates of a dimension are, the greater the amount of co-variability among the original variables this dimension explains. The results were presented graphically as plots with each dimension and length represented the relationship and weight to the principal components, correspondingly. We applied PCA using R software⁴¹ on our data set for which four variables had been determined: salinity, temperature, σ_θ , and ¹³⁷Cs activity concentrations from the surface layer to a depth of 400 m. The oceanographic context is then used to interpret the meaning of each dimension.

Results

Surface water properties and the distribution of ¹³⁴Cs and ¹³⁷Cs. Surface water samples were obtained from depths of less than 5 m, with temperatures of 9.7–34.9 °C and salinities of 21.8–34.2 psu (Figs. 2 and 3a). Salinity, TA, and σ_θ displayed large variations in surface waters (Fig. 3). Salinities were comprised between 35 and 21 psu and σ_θ was usually lower than 24 kg m⁻³ (Fig. 3a,b), indicating mixing between seawater and fresh water. The average TA in surface waters was 2243 ± 38 μmol kg⁻¹. NTA values associated with low σ_θ values, i.e., surface waters, deviated significantly from the average value determined in subsurface and deep waters (2309 μmol kg⁻¹) (Fig. 3d), implying that TA values in surface waters were likely to be affected by additional river TA sources.

In our samples, ¹³⁴Cs activity concentrations were under the detection limit (0.5 Bq m⁻³), and ¹³⁷Cs activity concentrations ranged from 0.5 to 2.0 Bq m⁻³ (Fig. 3e,f), with an average of 1.2 ± 0.3 Bq m⁻³ in the surface water (Supplementary Fig. S1). We also noticed a peak in the surface water ¹³⁷Cs vertical profile (Fig. 3f), with the maximum value ranging from 1.95 to 1.96 Bq m⁻³ (σ_θ = 18.8 to 21.4 kg m⁻³).

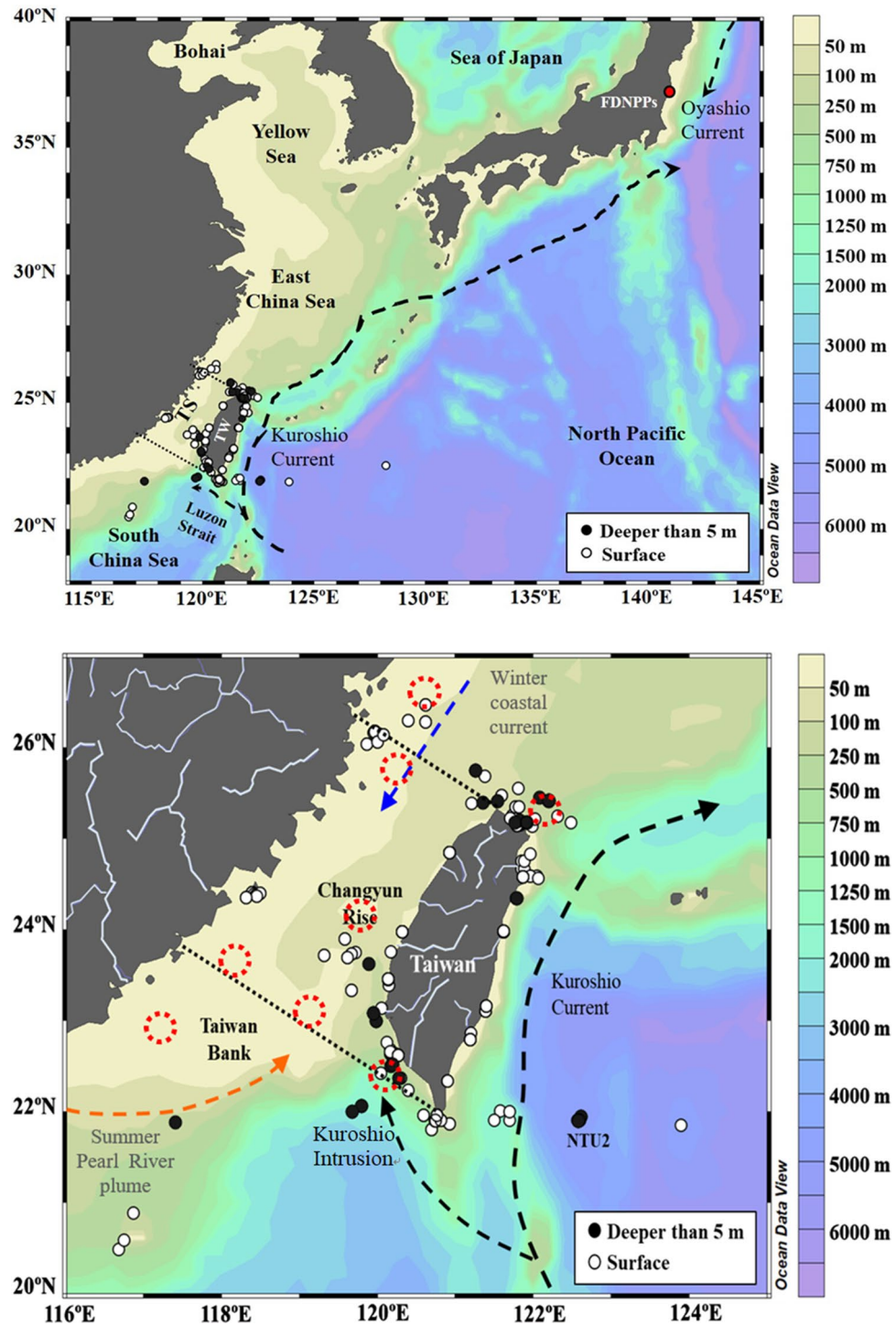


Figure 1. Sampling area. The Taiwan Strait and the Kuroshio east of Taiwan are critical regions in the western North Pacific Ocean (NPO). (a) Surface (solid markers) and subsurface and deep-water (open markers) samples were collected in the study area from 2018 to 2019. (b) The two dashed lines indicate the northern and southern boundaries of the Taiwan Strait used in this study. Red dashed circles are potential upwelling sites positioned using the temperature and chlorophyll-a data by Liu et al.³¹. This image was created by Ocean Data View (Version 4.7.5) (Schlitzer, R., Ocean Data View, <https://odv.awi.de>, 2016).

We arbitrarily divided the study area into geographic sectors and listed the average ¹³⁷Cs values for each sector in Table 1. The average values of ¹³⁷Cs activity concentrations in each sector were similar, with ¹³⁷Cs = 1.2 ± 0.3 Bq m⁻³ in the Taiwan Strait and 1.2 ± 0.2 Bq m⁻³ in the Kuroshio and its adjacent waters (Table 1).

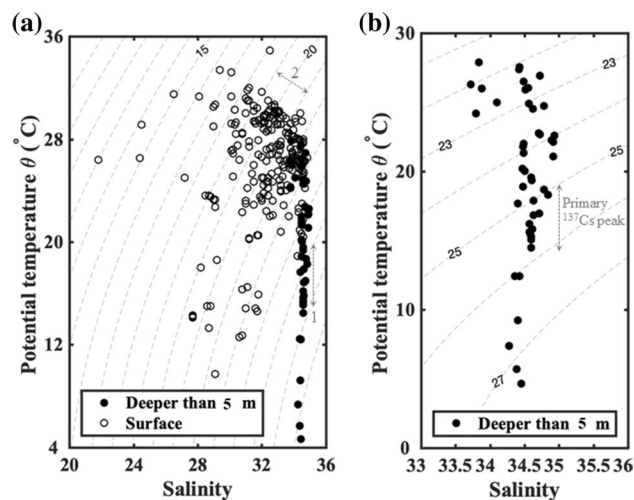


Figure 2. Temperature and salinity diagram. (a) Surface waters showed large variations in temperature and salinity. (b) Deep waters demonstrated salinities higher than 33.5 and represent the σ_θ range of the Subtropical Mode Water (STMW) and Central Mode Water (CMW) (25.1–26.2 kg m^{-3}). Labels “1” and “2” in (a) represent the σ_θ range of primary and secondary ^{137}Cs peaks, respectively.

In the surface waters, the ^{137}Cs values binned in one-degree latitude bands were higher between 25 to 26° N than the ones between 21 to 22° N in the Kuroshio and its adjacent waters (approximately to the east of 121° E in our study area) (Fig. 4a). Binned ^{137}Cs activity concentrations were close to each other to the west of 121° E (Fig. 4b).

The sea surface temperature (SST) distribution in 2018 displayed a general pattern, where SST values of less than 25 °C were found in the southern ECS and the northern Taiwan Strait while SST values over 27 °C were common for the Kuroshio and the Luzon Strait (Fig. 5). The SST in the northern Taiwan Strait and southern ECS showed strong seasonal variations, displaying SST over 25 °C during the summer-like months (i.e., July–September) and less than 25 °C during winter-like months (i.e., January–March) (Supplementary Fig. S2). The SST in shelf waters of the northern Taiwan Strait displayed stronger seasonal variations than those in the pelagic Kuroshio waters east of Taiwan.

In the shelf waters, including the Taiwan Strait and the waters off northern Taiwan, the average ^{137}Cs activity concentration was statistically higher in August than in February (two-tailed *t*-test, $p < 0.05$) (Fig. 6a). A statistically significant relationship was observed between monthly variations of ^{137}Cs and temperature (Fig. 6b). Monthly values of ^{137}Cs (Fig. 6a) increased from winter to summer and again started to decrease in fall, implying a seasonal cycle of ^{137}Cs in surface shelf waters.

Subsurface and deep water properties and distributions of ^{134}Cs and ^{137}Cs . Subsurface/deep water samples were taken from depths of 5–1000 m, with temperatures of 4.7–28.2 °C, and salinities over 21.0 to 34.0 psu (Fig. 2). The T–S characteristics of the subsurface and deep waters (Fig. 2b) of the Kuroshio-influenced region of the NPO covered the signals of STMW (σ_θ : ~25.6 kg m^{-3}), Kuroshio Tropical Water (KTW, $T = 17.0$ °C, $S = 34.6$ psu), and CMW (σ_θ ~26.1 kg m^{-3}). TA values in the subsurface and deep waters varied in a narrow range (Fig. 3c). The average and standard deviation of NTA value for waters between 5 to 400 m was 2309 ± 5 $\mu\text{mol kg}^{-1}$ (Fig. 3d).

At station NTU2 in the Kuroshio region, ^{134}Cs activities were below the detection limit (0.5 Bq m^{-3}), and ^{137}Cs activities were lower than 2.5 Bq m^{-3} from the surface to a depth of 1000 m (Fig. 3e). Moreover, two layers of elevated ^{137}Cs activities were observed: ^{137}Cs activities were mostly higher than 1 Bq m^{-3} from 0 to 400 m and also higher than 2 Bq m^{-3} from 200 to 400 m. By contrast, they were lower than 1 Bq m^{-3} from 600 to 1000 m (Fig. 3f). A synthesis of these results showed that low ^{137}Cs activity concentrations (1.5 to 0.6 Bq m^{-3}) corresponded to the high σ_θ (>25 kg m^{-3}) waters between 400 and 1000 m (Fig. 3e,f).

Discussion

The first three dimensions of the PCA results explained 91% of all variations, including sample temperature, salinity, and σ_θ , and ^{137}Cs activity concentration above the depth of 400 m. Dimension 1 explained 54% of the variations (Fig. 7a,b) and was dominated by σ_θ , temperature, and salinity (Table 2). σ_θ , salinity, and ^{137}Cs were positively correlated with Dimension 1 while the temperature was negatively correlated (Fig. 7a). We suggest that Dimension 1 represents density-induced water layer distributions and explains the primary peak of ^{137}Cs in the deep waters. This suggestion is consistent with the fact that σ_θ is positively correlated with the variables that have a high loading on Dimension 1 (Fig. 7c) and is a marker for the two layers of elevated ^{137}Cs in the top 400 m of the water column.

The highest coordinate of Dimension 2 corresponds to the secondary peak of ^{137}Cs in the surface waters (Fig. 7d), implying that Dimension 2 represents a factor that led to the secondary ^{137}Cs peak. The plot of Dimension 2 coordinates against σ_θ (Fig. 7d) can be divided into a high σ_θ (>22 kg m^{-3}) arm and a low σ_θ (<22 kg m^{-3})

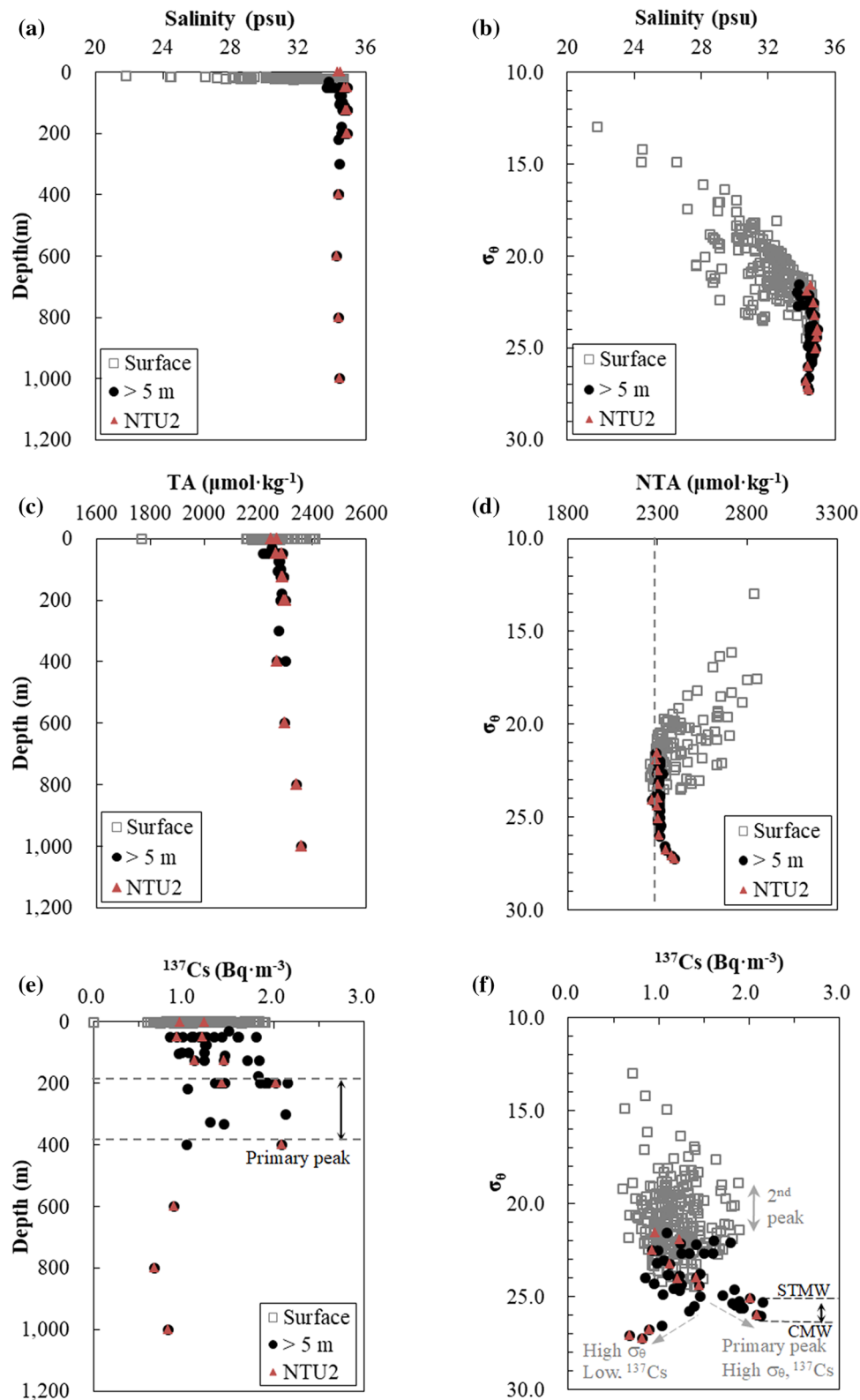


Figure 3. Vertical distributions of salinity, TA, NTA, and ^{137}Cs concentration. In the subsurface and deep waters, where (a) salinities varied from 33.7 to 34.9 long the vertical profile, (b) TA values varied from 2284 to 2360 $\mu\text{mol kg}^{-1}$, (c) ^{137}Cs activity concentrations displayed the primary peak at a depth range of 200–400 m, and where (d) σ_θ varied from 25.2 to 26.1 kg m^{-3} , (e) NTA was $2309 \pm 5 \mu\text{mol kg}^{-1}$, (f) the primary peak of ^{137}Cs was observed. (d) NTA with low σ_θ values deviated from 2309 in the near-surface waters. (f) The secondary peak of ^{137}Cs activity concentration displayed σ_θ ranging from 19 to 22 kg m^{-3} in the near-surface waters. All panels share the same legend. Data from NTU2 were noted with triangle markers in corresponding solid circles.

Sub-division	¹³⁷ Cs	
	Mean	STD ^a
Taiwan strait	1.2	0.3
KC and adjacent water	1.2	0.2

Table 1. Average ¹³⁷Cs values for the Taiwan Strait and the Kuroshio Current (KC) east of Taiwan (2018–2019) in Bq m⁻³. ^aSTD represents the standard deviation of the corresponding mean values.

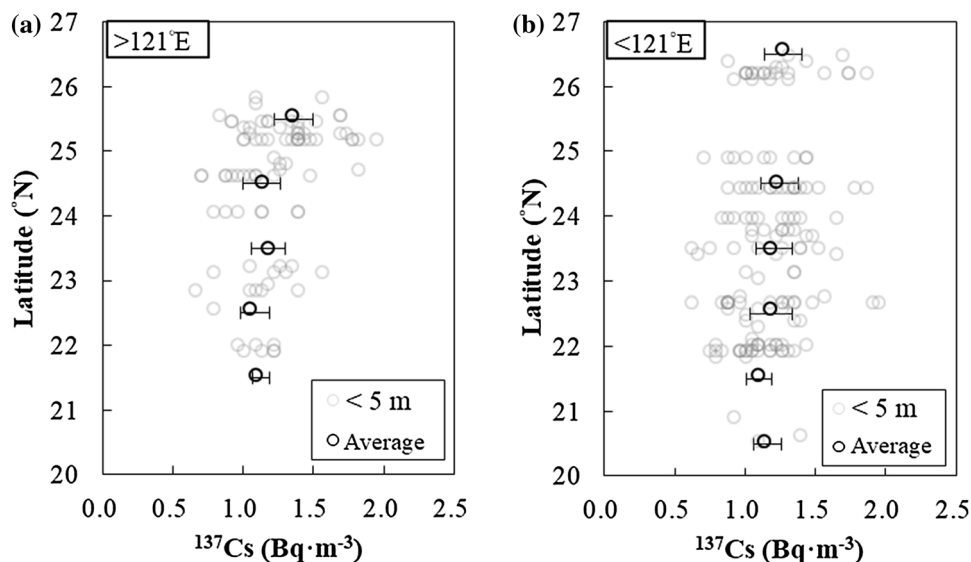


Figure 4. Latitude to ¹³⁷Cs relationships in the near-surface waters. To the east of 121° E (a), the binned ¹³⁷Cs activity concentration in one-degree latitude bands from 25 to 26° N was higher than the one from 21 to 22° N (black squares). (b) The binned ¹³⁷Cs values in each latitude were close to each other to the west of 121° E.

arm. As both temperature and salinity were positively correlated with Dimension 2 (Fig. 7a, Table 2), we hypothesize that the high σ_θ arm was caused by upwelling which transports high salinity water toward the surface and reduces the thickness of the lens of warm surface water in this study area. Upwelling near the coast of Taiwan and in the Taiwan Strait is known to transport subsurface waters (as deep as 80 m to 100 m) to the near-surface layer. The vertical velocity of upwelling off northeastern Taiwan (Fig. 1)^{42–45} has been estimated to be 15 m day⁻¹ on the shelf and over 40 m day⁻¹ at the shelf edge^{29,46}. The σ_θ of water with salinity = 34.3 psu, temperature = 18.3 °C, and $\sigma_\theta = 25.0$ kg m⁻³ at a depth of 200 m, can decrease to less than 22 kg m⁻³ if the water temperature increases to 28 °C at 1 m during the upwelling process (Fig. 2a). This annual upwelling to the northeastern Taiwan may lead to the higher binned ¹³⁷Cs between 25 and 26° N than the others to the east of 121°E in the near-surface waters (Fig. 4a). Another driving force of annual upwelling is internal tide, which can induce upwelling in the waters off northeastern Taiwan⁴⁷ and off southern Taiwan^{48–50}. Moreover, this transition σ_θ of 22 kg m⁻³ in Fig. 7d was also consistent with the transition range of σ_θ where NTA positively deviated from 2309 ± 5 $\mu\text{mol kg}^{-1}$ in the near-surface water (Fig. 3d). This deviation of NTA in low σ_θ waters indicates freshwater inputs from terrestrial runoff. To sum up, we suggest that mixing between riverine freshwater and seawater is responsible for the lower σ_θ arm while upwelling drives the higher σ_θ arm in Fig. 7d.

Dimension 3 accounted for no more of the variance than ¹³⁷Cs itself (Table 2, Fig. 7b), suggesting that it was controlled by the chemical characteristics of ¹³⁷Cs. MacKenzie et al.⁵¹ have argued that high freshwater discharge from land can remobilize ¹³⁷Cs from surface sediments (< 10 cm). Future work should be conducted towards a dynamic representation of radionuclide transfer among freshwater, seawater, sediment, and the biological compartments¹¹.

The seasonal variation of the ¹³⁷Cs activity concentration in the Taiwan Strait (Fig. 6a) reflects the seasonal intrusions of waters from Kuroshio intrusion, ECS, and SCS. Wu et al.¹⁹ corrected their ¹³⁷Cs activity concentrations to the same date as this study, leading to a mean of 0.71 ± 0.27 Bq m⁻³ in the surface ECS and an average of 0.92 ± 0.28 Bq m⁻³ in the surface SCS. These results are consistent with our observation that southward-flowing cold waters with low ¹³⁷Cs values intruded into the northern half of the shallow Taiwan Strait during the winter while the reverse took place during the summer (Fig. 6a)^{22,24,25}. In addition to the Kuroshio offshoot transporting warm waters with higher ¹³⁷Cs values in the summer, the Pearl river plume can also intrude into the southern Taiwan Strait during the summer⁵². It follows that the slightly lower ¹³⁷Cs activity concentration during July

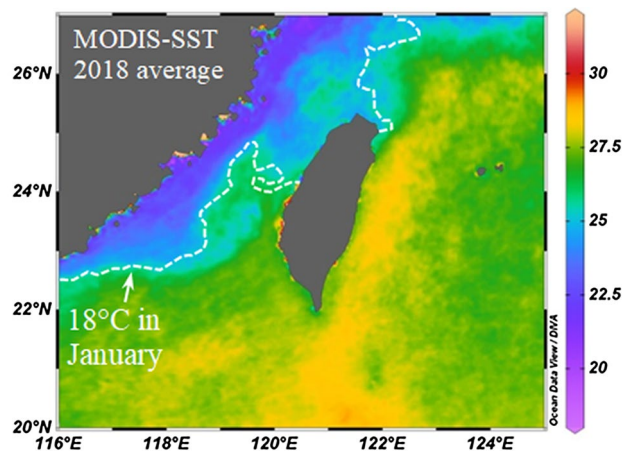


Figure 5. Sea surface distributions of seawater temperature. SST is an important factor while understanding the oceanic condition. High SST (MODIS 2018) was detected in the Kuroshio east of Taiwan and its intrusion into the southeastern Taiwan Strait. Low SST was identified along the coastline from the East China Sea (ECS) to the western side of the Taiwan Strait. The white dashed line indicates the contour line of 18 °C obtained from January. Monthly SST data was collected from AQUA-MODIS with a spatial resolution of $1^{\circ} \times 1^{\circ}$ (<https://neo.sci.gsfc.nasa.gov/view.php?datasetId=MYD28M>). This data was accessed on July 3, 2021. This image was created by Ocean Data View (Version 4.7.5) (Schlitzer, R., Ocean Data View, <https://odv.awi.de>, 2016).

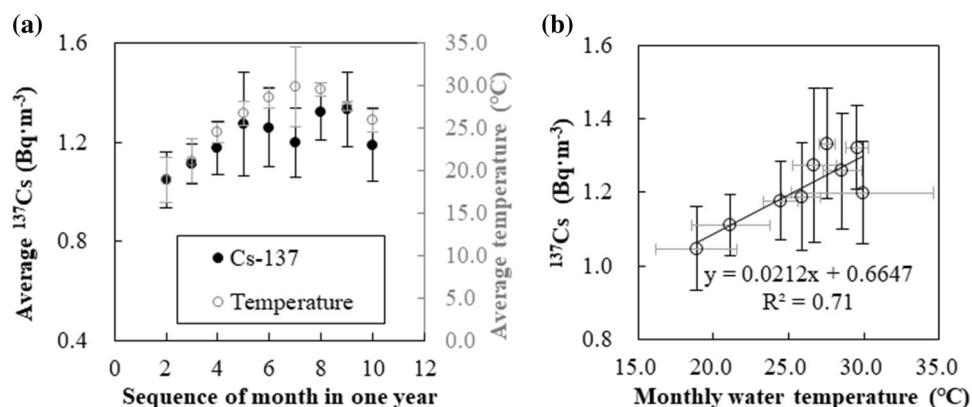


Figure 6. Monthly variations in sea-surface ^{137}Cs activity concentration in the Taiwan Strait and southern ECS. (a) ^{137}Cs activity concentration and corresponding seawater temperature were measured at the study sites on both sides of the Taiwan Strait and the waters off northern Taiwan (refer to Fig. 1b). Both parameters displayed seasonal variations: low in winter and high in summer. (b) The monthly ^{137}Cs activity concentration was statistically correlated to its corresponding seawater temperature.

indicates that the effect of the intrusion of Kuroshio is more than offset by the amount of warm water with lower ^{137}Cs activity originating from the SCS.

The maximum in ^{137}Cs activity concentration was observed in a specific range of σ_{θ} in the subsurface and deep waters (Fig. 3e,f), implying a lateral transport along the 125–400 m depth horizon in addition to local atmospheric fallout. Local and modern atmospheric ^{137}Cs fallout can only affect the average ^{137}Cs values in the surface waters (Table 1). ^{137}Cs activity concentrations in the subsurface water of the study area displayed characteristics ($\sigma_{\theta} = 25.2$ and 26.1 kg m^{-3}) which were similar to those of STMW and CMW ($\sigma_{\theta} = 25.3$ to 26.3 kg m^{-3}) in NPO⁴ (Fig. 3). Some surface NTA values and also the average NTA value in subsurface waters ($2309 \pm 5 \mu\text{mol kg}^{-1}$) of this study were consistent with NTA values previously reported in the surface western NPO (2301 ± 9 to $2299 \pm 5.4 \mu\text{mol kg}^{-1}$)^{53,54}. The maximum ^{137}Cs activity concentration at a depth of 300 to 400 m at 165°E before the FDNPP event should be 1.65 Bq m^{-3} (corrected to January 1st, 2020)³. After the FDNPP event in June/July 2012, ^{137}Cs activity concentrations at depths of between 0 and 600 m in the western NPO (25 to 45°N , 165°E) were between 2.1 and higher than 8.4 Bq m^{-3} (corrected to January 1st, 2020)⁴. As the half-life of ^{134}Cs is shorter than that of ^{137}Cs , $^{134}\text{Cs}/^{137}\text{Cs}$ is assumed to be 1.000 at 165°E ; it became 0.095 after 7.5 year (July 2012 to December 2020). Since ^{137}Cs activity concentration is already low ($< 2.1 \text{ Bq m}^{-3}$) in this study area, ^{134}Cs is expected to be $< 0.2 \text{ Bq m}^{-3}$ which is lower than the detection limit (0.5 Bq m^{-3}) in this study.

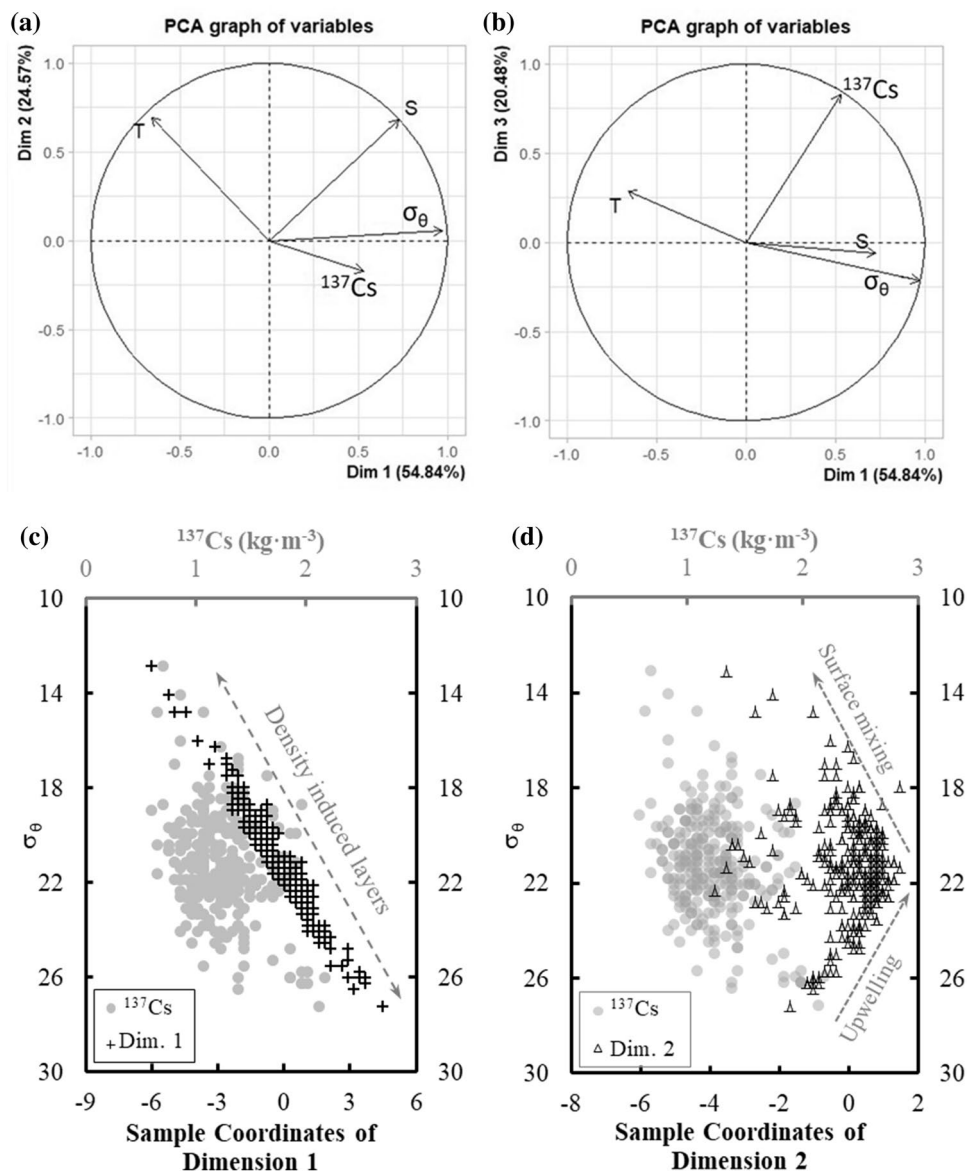


Figure 7. Results of principal component analysis (PCA) and sample coordinates. (a,b) σ_θ dominated variations in Dimension 1; increasing temperature and salinity dominated variations in Dimension 2; and ^{137}Cs dominated variations in Dimension 3. (c) The coordinates of individual results in Dimension 1 were consistent with the primary peak of ^{137}Cs defined along the stratified water column. (d) The peak coordinate of Dimension 2 was consistent with the secondary ^{137}Cs peak along the σ_θ gradient.

	Dim. 1	Dim. 2	Dim. 3
Temperature	-0.659	0.696	0.284
Salinity	0.728	0.682	-0.061
σ_θ	0.974	0.055	-0.213
^{137}Cs activity	0.530	-0.174	0.830

Table 2. Principal components.

The increase between the estimated ^{137}Cs activity concentration before FDNPP (1.65 Bq m^{-3}) and the maximum measured ^{137}Cs value after FDNPP (2.1 Bq m^{-3}) in this study (both corrected to January 1st, 2020) implies an additional ^{137}Cs activity concentration of $2.1 - 1.65 = 0.45 \text{ Bq m}^{-3}$ during this time period. This increase is the result of complex physical transportation from NPO to the study area. Kamidaira et al.⁵⁵ reported that approximately 43% of FDNPP-derived ^{137}Cs could be delivered to below the mixed layer through eddy processes. In

addition, ^{137}Cs in STMW and CMW appears to be transported clockwise toward the western boundary of the NPO^{3,56–59}. This subsurface or deep-water layer corresponding to $\sigma_\theta = 26.7 \text{ kg m}^{-3}$ can further rise westward and reach the shelf break surrounding Taiwan^{60–66}. East of Taiwan, the Kuroshio is a swift and powerful current that can reach as deep as 400–600 m⁶⁷. While the primary ^{137}Cs maximum centered around σ_θ of 25.3 to 26.1 kg m^{-3} is suspected to be from lateral transportation from the NPO, there is still a research gap between pelagic studies in the NPO and shelf break data in this study area. For example, impacts of interleaving⁶⁸ and meso-scale eddies⁶⁹ on the cross-Kuroshio transport mechanism of ^{137}Cs are still unclear. Direct evidence to constrain the origin and evolution of the ^{137}Cs maxima along 165° E to this study area is needed in the future. We suggest integrating multiple chemical tracers to study the complex circulation across the pelagic NPO to its western shelf boundary in the future.

Received: 7 July 2021; Accepted: 2 November 2021

Published online: 17 November 2021

References

1. Aarkrog, A. Input of anthropogenic radionuclides into the World Ocean. *Deep. Res. Part II Top. Stud. Oceanogr.* **50**, 2597–2606 (2003).
2. Aoyama, M., Hirose, K. & Igarashi, Y. Re-construction and updating our understanding on the global weapons tests ^{137}Cs fallout. *J. Environ. Monit.* **8**, 431–438 (2006).
3. Aoyama, M., Hirose, K., Nemoto, K., Takatsuki, Y. & Tsumune, D. Water masses labeled with global fallout ^{137}Cs formed by subduction in the North Pacific. *Geophys. Res. Lett.* **35**, 1–6 (2008).
4. Aoyama, M. *et al.* ^{134}Cs and ^{137}Cs in the North Pacific Ocean derived from the March 2011 TEPCO Fukushima Dai-ichi Nuclear Power Plant accident, Japan. Part one: Surface pathway and vertical distributions. *J. Oceanogr.* **72**, 53–65 (2016).
5. Aoyama, M. *et al.* ^{134}Cs and ^{137}Cs in the North Pacific Ocean derived from the March 2011 TEPCO Fukushima Dai-ichi Nuclear Power Plant accident, Japan. Part two: Estimation of ^{134}Cs and ^{137}Cs inventories in the North Pacific Ocean. *J. Oceanogr.* **72**, 53–65 (2016).
6. Buesseler, K. *et al.* Fukushima Daiichi-Derived radionuclides in the ocean: Transport, fate, and impacts. *Ann. Rev. Mar. Sci.* **9**, 173–203 (2017).
7. Inomata, Y., Aoyama, M., Hamajima, Y. & Yamada, M. Transport of FNPP1-derived radiocaesium from subtropical mode water in the western North Pacific Ocean to the Sea of Japan. *Ocean Sci.* **3**, 813–826 (2018).
8. Mathieu, A. *et al.* Fukushima Daiichi-derived radionuclides in the atmosphere, transport and deposition in Japan: A review. *Appl. Geochem.* **91**, 122–139 (2018).
9. Smith, J. N. *et al.* Recent transport history of Fukushima Radioactivity in the Northeast Pacific Ocean. *Environ. Sci. Technol.* **51**, 10494–10502 (2017).
10. Smith, J. N. *et al.* Arrival of the Fukushima radioactivity plume in North American continental waters. *Proc. Natl. Acad. Sci.* **112**, 1310–1315 (2015).
11. Vives i Batlle, J. *et al.* Marine radioecology after the Fukushima Dai-ichi nuclear accident: Are we better positioned to understand the impact of radionuclides in marine ecosystems?. *Sci. Total Environ.* **618**, 80–92 (2018).
12. Aoyama, M., Tsumune, D., Inomata, Y. & Tateda, Y. Mass balance and latest fluxes of radiocaesium derived from the Fukushima accident in the western North Pacific Ocean and coastal regions of Japan. *J. Environ. Radioact.* **217**, 106206 (2020).
13. Inomata, Y., Aoyama, M., Tsubono, T., Tsumune, D. & Hirose, K. Spatial and temporal distributions of ^{134}Cs and ^{137}Cs derived from the TEPCO Fukushima Daiichi Nuclear Power Plant accident in the North Pacific Ocean by using optimal interpolation analysis. *Environ. Sci. Process. Impacts* **18**, 126–136 (2016).
14. Tsubono, T. *et al.* Evaluation of radioactive cesium impact from atmospheric deposition and direct release fluxes into the North Pacific from the Fukushima Daiichi nuclear power plant. *Deep Sea Res. Part I Oceanogr. Res. Pap.* **115**, 10–21 (2016).
15. Kumamoto, Y. *et al.* Radiocaesium in the western subarctic area of the North Pacific Ocean, Bering Sea, and Arctic Ocean in 2013 and 2014. *Appl. Radiat. Isot.* **126**, 88–92 (2017).
16. Hanawa, K. & Talley, D. L. Chapter 5.4 Mode waters. *Int. Geophys.* **77**, 373–386 (2001).
17. Oka, E. & Suga, T. Formation region of North Pacific subtropical mode water in the late winter of 2003. *Geophys. Res. Lett.* **30**, 10–13 (2003).
18. McCartney, M. The subtropical recirculation of mode waters. *J. Mar. Res.* **40**, 427–464 (1982).
19. Oka, E. & Suga, T. Differential formation and circulation of North Pacific Central Mode Water. *J. Phys. Oceanogr.* **35**, 1997–2011 (2005).
20. Suga, T., Takei, Y. & Hanawa, K. Thermostad distribution in the North Pacific subtropical gyre: The central mode water and the subtropical mode water. *J. Phys. Oceanogr.* **27**, 140–152 (1997).
21. Wu, J., Xiao, X. & Sun, J. Distribution and budget of ^{137}Cs in the China Seas. *Sci. Rep.* **10**, 1–15 (2020).
22. Jan, S., Wang, J., Chern, C. S. & Chao, S. Y. Seasonal variation of the circulation in the Taiwan Strait. *J. Mar. Syst.* **35**, 249–268 (2002).
23. Kuo, N. J. & Ho, C. R. ENSO effect on the sea surface wind and sea surface temperature in the Taiwan Strait. *Geophys. Res. Lett.* **31**, 10–13 (2004).
24. Jan, S., Tseng, Y.-H. & Dietrich, D. E. Sources of water in the Taiwan Strait. *J. Oceanogr.* **66**, 211–221 (2010).
25. Chang, Y., Lee, K., Lee, M. & Lan, K. Satellite observation on the exceptional intrusion of cold water in the Taiwan Strait. *Terr. Atmos. Ocean. Sci.* **20**, 661–669 (2009).
26. Liu, J. T. *et al.* A comprehensive sediment dynamics study of a major mud belt system on the inner shelf along an energetic coast. *Sci. Rep.* **8**, 1–14 (2018).
27. Huang, T. H., Chen, C. T. A., Bai, Y. & He, X. Elevated primary productivity triggered by mixing in the quasi-cul-de-sac Taiwan Strait during the NE monsoon. *Sci. Rep.* **10**, 1–9 (2020).
28. Chang, Y.-L. & Oey, L.-Y. Why can wind delay the shedding of loop current eddies?. *J. Phys. Ocean.* **40**, 2481–2495 (2010).
29. Liu, K.-K. *et al.* Response of Kuroshio upwelling to the onset of the northeast monsoon in the sea north of Taiwan: Observations and a numerical simulation. *J. Geophys. Res.* **97**, 12511–12526 (1992).
30. Lee, M. A., Kuo, Y. C., Chan, J. W., Chen, Y. K. & Teng, S. Y. Long-term (1982–2012) summertime sea surface temperature variability in the Taiwan strait. *Terr. Atmos. Ocean. Sci.* **29**, 183–192 (2015).
31. Liu, J. T. *et al.* Three-dimensional coupling between size-fractionated chlorophyll-a, POC and physical processes in the Taiwan Strait in summer. *Prog. Oceanogr.* **176**, 102129 (2019).
32. Shu, Y. *et al.* The contribution of local wind and ocean circulation to the interannual variability in coastal upwelling intensity in the Northern South China Sea. *J. Geophys. Res. Ocean.* **123**, 6766–6778 (2018).

33. Gan, J., Cheung, A., Guo, X. & Li, L. Intensified upwelling over a widened shelf in the northeastern South China Sea. *J. Geophys. Res. Ocean.* **114**, 1–15 (2009).
34. Huang, W.-J., Kao, K.-J., Lin, Y.-S., Arthur Chen, C.-T. & Liu, J. T. Daily to weekly impacts of mixing and biological activity on carbonate dynamics in a large river-dominated shelf. *Estuar. Coast. Shelf Sci.* **245**, 106914 (2020).
35. Feldman, C. & Rains, T. C. The collection and flame photometric determination of Cesium. *Anal. Chem.* **36**, 405–409 (1964).
36. Krishnamoorthy, T. M., Doshi, G. R. & Sastry, V. N. Exchange capacity of ammonium phosphomolybdate for caesium by batch technique. *Curr. Sci.* **40**, 542–544 (1971).
37. Huang, W.-J., Wang, Y. & Cai, W.-J. Assessment of sample storage techniques for total alkalinity and dissolved inorganic carbon in seawater. *Limnol. Oceanogr. Methods* **10**, 711–717 (2012).
38. Chen, G.-T. & Millero, F. J. Gradual increase of oceanic CO₂. *Nature* **277**, 205–206 (1979).
39. Pearson, K. LIII. On lines and planes of closest fit to systems of points in space. *Lond. Edinb. Dublin Philos. Mag. J. Sci.* **2**, 559–572 (1901).
40. Jolliffe, I. T. Principal components in regression analysis. In *Principal Component Analysis* (ed. Jolliffe, I. T.) 129–155 (Springer, 1986). https://doi.org/10.1007/978-1-4757-1904-8_8.
41. Husson, F., Pagès, J. & Lê, S. In *Exploratory Multivariate Analysis by Example Using R*. Chapman & Hall/CRC Computer Science & Data Analysis, pp. 240, 2010, (CRC Press Taylor & Francis, 2017).
42. Wu, C. R., Lu, H. F. & Chao, S. Y. A numerical study on the formation of upwelling off northeast Taiwan. *J. Geophys. Res. Ocean.* **113**, 1–12 (2008).
43. Shen, M.-L., Tseng, Y.-H. & Jan, S. The formation and dynamics of the cold-dome off northeastern Taiwan. *J. Mar. Syst.* **86**, 10–27 (2011).
44. Tsai, Y., Chern, C.-S., Jan, S. & Wang, J. Numerical study of cold dome variability induced by Typhoon Morakot (2009) off northeastern Taiwan. *J. Mar. Res.* **71**, 109–131 (2013).
45. Yin, W. & Huang, D. Short-term variations in the surface upwelling off northeastern Taiwan observed via satellite Data. *J. Geophys. Res. Ocean.* **124**, 939–954 (2019).
46. Chang, Y. L., Oey, L. Y., Wu, C. R. & Lu, H. F. Why are there upwellings on the northern shelf of Taiwan under northeasterly winds?. *J. Phys. Oceanogr.* **40**, 1405–1417 (2010).
47. Chang, H. et al. Generation and propagation of M2 internal tides modulated by the Kuroshio northeast of Taiwan. *J. Geophys. Res. Ocean.* **124**, 2728–2749 (2019).
48. Pai, S. C., Wei, C. L., Lin, S., Wen, L. S. & Tseng, C. M. Observation of internal tide-induced nutrient upwelling in Hungtsai Trough, a submarine canyon in the northern South China Sea. *Cont. Shelf Res.* **120**, 59–67 (2016).
49. Hu, C. K. et al. Numerical simulation of barotropic tides around Taiwan. *Terr. Atmos. Ocean. Sci.* **21**, 71–84 (2010).
50. Jan, S. & Chen, C. T. A. Potential biogeochemical effects from vigorous internal tides generated in Luzon Strait: A case study at the southernmost coast of Taiwan. *J. Geophys. Res. Ocean.* **114**, 1–14 (2009).
51. MacKenzie, A. B., Cook, G. T., McDonald, P. & Jones, S. R. The influence of mixing timescales and re-dissolution processes on the distribution of radionuclides in northeast Irish Sea sediments. *J. Environ. Radioact.* **39**, 35–53 (1998).
52. Bai, Y. et al. Intrusion of the Pearl River plume into the main channel of the Taiwan Strait in summer. *J. Sea Res.* **95**, 1–15 (2015).
53. Jiang, Z.-P., Tyrrell, T., Hydes, D. J., Dai, M. & Hartman, S. E. Variability of alkalinity and the alkalinity–salinity relationship in the tropical and subtropical surface ocean. *Glob. Biogeochem. Cycles* **28**, 729–742 (2014).
54. Takatani, Y. et al. Relationships between total alkalinity in surface water and sea surface dynamic height in the Pacific Ocean. *J. Geophys. Res. Ocean.* **119**, 2806–2814 (2014).
55. Kamidaira, Y., Uchiyama, Y., Kawamura, H., Kobayashi, T. & Furuno, A. Submesoscale mixing on initial dilution of radionuclides released from the Fukushima Daiichi Nuclear Power Plant. *J. Geophys. Res. Ocean.* **123**, 2808–2828 (2018).
56. Kaeriyama, H. et al. Southwest intrusion of ¹³⁴Cs and ¹³⁷Cs derived from the Fukushima Dai-ichi nuclear power plant accident in the western North Pacific. *Environ. Sci. Technol.* **48**, 3120–3127 (2014).
57. Kaeriyama, H. et al. Intrusion of Fukushima-derived radiocaesium into subsurface water due to formation of mode waters in the North Pacific. *Sci. Rep.* **6**, 1–10 (2016).
58. Men, W. et al. Radioactive status of seawater in the northwest Pacific more than one year after the Fukushima nuclear accident. *Sci. Rep.* **5**, 1–9 (2015).
59. Oka, E. & Qiu, B. Progress of north pacific mode water research in the past decade. *New Dev. Mode-Water Res. Clim. Eff.* <https://doi.org/10.1007/s10872-011-0032-5> (2013).
60. Chen, C. T. A., Ruo, R., Paid, S. C., Liu, C. T. & Wong, G. T. F. Exchange of water masses between the East China Sea and the Kuroshio off northeastern Taiwan. *Cont. Shelf Res.* **15**, 19–39 (1995).
61. Chen, C. T. A. The Kuroshio intermediate water is the major source of nutrients on the East China Sea continental shelf. *Oceanol. Acta* **19**, 523–527 (1996).
62. Jan, S. et al. Mean structure and variability of the cold dome northeast of Taiwan. *Oceanography* **24**, 100–109 (2011).
63. Gopalakrishnan, G., Cornuelle, B. D., Gawarkiewicz, G. & McClean, J. L. Structure and evolution of the cold dome off northeastern Taiwan: A numerical study. *Oceanography* **26**, 66–79 (2013).
64. Hsin, Y. C., Qiu, B., Chiang, T. L. & Wu, C. R. Seasonal to interannual variations in the intensity and central position of the surface Kuroshio east of Taiwan. *J. Geophys. Res. Ocean.* **118**, 4305–4316 (2013).
65. Nakamura, H. et al. Intermediate and deep water formation in the Okinawa trough. *J. Geophys. Res. Ocean.* **118**, 6881–6893 (2013).
66. Yan, X., Zhu, X.-H., Pang, C. & Zhang, L. Effects of mesoscale eddies on the volume transport and branch pattern of the Kuroshio east of Taiwan. *J. Geophys. Res. Ocean.* **121**, 7683–7700 (2016).
67. Jan, S. et al. Large variability of the Kuroshio at 23.75° N east of Taiwan. *J. Geophys. Res. C Ocean.* **120**, 1825–1840 (2015).
68. Jan, S., Wang, S. H., Yang, K. C., Yang, Y. J. & Chang, M. H. Glider observations of interleaving layers beneath the Kuroshio primary velocity core east of Taiwan and analyses of underlying dynamics. *Sci. Rep.* **9**, 1–11 (2019).
69. Jan, S., Mensah, V., Andres, M., Chang, M. H. & Yang, Y. J. Eddy-Kuroshio interactions: Local and remote effects. *J. Geophys. Res. Ocean.* **122**, 9744–9764 (2017).

Acknowledgements

The authors would like to thank government employees and contractors who helped in sampling seawater in the study area. The authors are also grateful to the chief scientists, captains, and technicians on R/Vs Ocean Research I, II, and III for their assistance. This study was funded by the Radiation Monitoring Center, Atomic Energy Council (Grant No. #107-0103 and 108-0103). Data are available in the supplementary file (Supplementary Table S1).

Author contributions

W.-J.H. analyzed the data and wrote the main manuscript and C.T.A.C. edited and supervised this project. M.T.L. coordinates and supervises this project and the sample analysis. K.C.H. prepared all figures and organized data. K.J.K. was involved in the discussion and collected samples. M.A.L. contribute satellite data. M.A.L.,

Y.J.Y., and S.J. edited this manuscript and collected samples. All authors designed the experiments and reviewed this manuscript.

Competing interests

The authors declare no competing interests.

Additional information

Supplementary Information The online version contains supplementary material available at <https://doi.org/10.1038/s41598-021-01895-y>.

Correspondence and requests for materials should be addressed to W.-J.H. or C.-T.A.C.

Reprints and permissions information is available at www.nature.com/reprints.

Publisher's note Springer Nature remains neutral with regard to jurisdictional claims in published maps and institutional affiliations.



Open Access This article is licensed under a Creative Commons Attribution 4.0 International License, which permits use, sharing, adaptation, distribution and reproduction in any medium or format, as long as you give appropriate credit to the original author(s) and the source, provide a link to the Creative Commons licence, and indicate if changes were made. The images or other third party material in this article are included in the article's Creative Commons licence, unless indicated otherwise in a credit line to the material. If material is not included in the article's Creative Commons licence and your intended use is not permitted by statutory regulation or exceeds the permitted use, you will need to obtain permission directly from the copyright holder. To view a copy of this licence, visit <http://creativecommons.org/licenses/by/4.0/>.

© The Author(s) 2021